Journal of proteome research

pubs.acs.org/jpr

Article

Prenatal and Early Postnatal Cerebral D-Aspartate Depletion Influences L-Amino Acid Pathways, Bioenergetic processes, and Developmental Brain Metabolism

Manuela Grimaldi, Carmen Marino, Michela Buonocore, Angelo Santoro, Eduardo Sommella, Fabrizio Merciai, Emanuela Salviati, Arianna De Rosa, Tommaso Nuzzo, Francesco Errico, Pietro Campiglia, Alessandro Usiello,* and Anna Maria D'Ursi*

Cite This: *J. Proteome Res.* 2021, 20, 727−739

Read Online

ACCESS | Metrics & More | Article Recommendations | Supporting Information

ABSTRACT: D-Amino acids were believed to occur only in bacteria and invertebrates. Today, it is well known that D-amino acids are also present in mammalian tissues in a considerable amount. In particular, high levels of free D-serine (D-Ser) and D-aspartate (D-Asp) are found in the brain. While the functions of D-Ser are well known, many questions remain unanswered regarding the role of D-Asp in the central nervous system. D-Asp is very abundant at the embryonic stage, while it strongly decreases after birth because of the expression of D-aspartate oxidase (*Ddo*) enzyme, which catalyzes the oxidation of this D-amino acid into oxaloacetate, ammonium, and hydrogen peroxide. Pharmacologically, D-Asp acts as an endogenous agonist of *N*-methyl D-aspartate and mGlu5 receptors, which are known to control fundamental brain processes, including brain development, synaptic plasticity, and cognition. In this work, we studied a recently generated knockin mouse model ($R26^{Ddo/Ddo}$), which was designed to express DDO beginning at the zygotic stage. This strategy enables D-Asp to be almost eliminated in both prenatal and postnatal lives. To understand which biochemical pathways are affected by depletion of D-Asp, in this study, we carried out a metabolomic and lipidomic study of *Ddo* knockin brains at different stages of embryonic and postnatal development, combining nuclear magnetic resonance (NMR) and high-resolution mass spectrometry (HRMS) techniques. Our study shows that D-Asp deficiency in the brain influences amino acid pathways such as threonine, glycine, alanine, valine, and glutamate. Interestingly, D-Asp is also correlated with metabolites involved in brain development and functions such as choline, creatine, phosphocholine (PCho), glycerophosphocholine (GPCho), sphingolipids, and glycerophospholipids, as well as metabolites involved in brain energy metabolism, such as GPCho, glucose, and lactate.

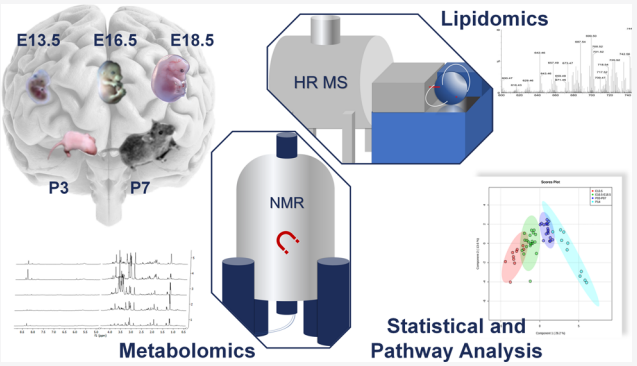

KEYWORDS: *NMR, HRMS, metabolomics, brain tissue*

INTRODUCTION

Free D-aspartate (D-Asp) is found in high amounts in the mammalian brain during prenatal and early postnatal life and dramatically decreases after birth[1−8] because of the activity of D-aspartate oxidase (DDO), the only known enzyme able to degrade D-Asp, by catalyzing its oxidation in oxaloacetate, ammonium, and hydrogen peroxide.[9−11] Interestingly, recent studies revealed that *Ddo* mRNA expression increases in the brain during postnatal life because of a progressive *Ddo* promoter demethylation, suggesting that epigenetic regulatory events at the *Ddo* promoter ultimately control DDO expression and activity and, in turn, the time-dependent variations of D-Asp levels.[1,4,12−14] Unlike the well-established D-Asp degrading enzyme, the specific mechanisms and enzymes governing the biosynthesis of this endogenous D-amino acid in mammals remain a matter of debate.[9] However, a role for serine racemase has been recently reported in the generation of this D-amino acid in specific rodent brain regions.[15,16]

Despite the considerable abundance of D-Asp in the embryonic phase, the biological role of D-Asp in brain development and function has not been fully elucidated.[17] In the last decade, D-Asp has been shown to act as an endogenous agonist of *N*-methyl D-aspartate (NMDA) and mGlu5 receptors.[6,18−21] In line with these pharmacological features, non-physiological higher D-Asp cerebral concentrations

Received: August 11, 2020
Published: December 4, 2020

https://dx.doi.org/10.1021/acs.jproteome.0c00622
J. Proteome Res. 2021, 20, 727−739

obtained by its exogenous administration or by *Ddo* knockout ($Ddo^{-/-}$) approach in mice have been reported to influence synapse morphology, synaptic plasticity, and cognition.[6−8,19,22]

Consistent with the pharmacological ability of D-Asp to stimulate NMDA receptors, studies in $Ddo^{-/-}$ mice and primary cortical neurons have demonstrated that persistently high levels of this D-amino acid induce severe neuroinflammation and neuronal cell death.[1,23−25]

Despite the findings above regarding the role of D-Asp in adulthood, the biological significance of high D-Asp content during brain development has not been elucidated. Hence, to fill this gap, we recently generated a genetically engineered knockin mouse, $R26^{Ddo/Ddo}$, characterized by embryonic overexpression of the *Ddo* gene and consequent depletion of cerebral D-Asp. In these animals, early cerebral D-Asp removal is associated with alteration in the number of parvalbumin-positive cortical interneurons and memory abilities.[4]

In the present work, we attempted to elucidate the metabolic influence of D-Asp during brain development. To this end, we analyzed brain tissue extracts of $R26^{Ddo/Ddo}$ and control $R26^{+/+}$ mice at different stages of embryonic and early postnatal brain development using nuclear magnetic resonance (NMR) spectroscopy and high-resolution mass spectrometry (HRMS). Notably, our results showed the dramatic impact of early cerebral D-Asp in modulating central biochemical pathways linked to cell bioenergetic processes, brain development and function, as well as L-amino acids and lipid metabolism.

MATERIALS AND METHODS

Animal Care and Protocol

$R26^{Ddo/+}$ mice were interbred to produce $R26^{+/+}$ and homozygous $R26^{Ddo/Ddo}$ animals. Mice were genotyped by PCR using the following primers: R26 wt Fw, 5′-CTG TGG ACA GAG GAG CCA TAA C-3′; R26 wt Rev, 5′-CTG TCT CTG CCT CCA GAG TGC T-3′; DdoLacZ Rev 5′-TGG ACT AAA CAC CGG TGC CC-3′. The wild-type fragment (316 bp) was generated by the primers R26 wt Fw and R26 wt Rev; the targeted fragment (490 bp) was generated by the primers R26 wt Fw and DdoLacZ Rev. Amplification conditions were 95 °C for 5 min; 35 cycles: 95 °C for 30 s, 62 °C for 30 s, 72 °C for 1 min; and 72 °C for 10 min. Animals were group housed (five per cage) at a constant temperature (22 ± 1 °C) on a 12 h light/dark cycle (lights on at 7 AM) with food and water ad libitum.

Mouse Tissue Collection

Metabolomic analysis was performed on whole brains of wild-type mice ($R26^{+/+}$) and knockin littermates ($R26^{Ddo/Ddo}$). We used both male and female animals. Whole brains were collected from $R26^{+/+}$ and $R26^{Ddo/Ddo}$ mice at different developmental stages, including the following time points: embryonic day (E) E13.5 ($n_{(R26^{+/+})} = 5$ and $n_{(R26^{Ddo/Ddo})} = 5$), E16.5 ($n_{(R26^{+/+})} = 5$ and $n_{(R26^{Ddo/Ddo})} = 5$), E18.5 ($n_{(R26^{+/+})} = 5$ and $n_{(R26^{Ddo/Ddo})} = 5$), postnatal day (P) P3 ($n_{(R26^{+/+})} = 4$ and $n_{(R26^{Ddo/Ddo})} = 4$) and P7 ($n_{(R26^{+/+})} = 5$ and $n_{(R26^{Ddo/Ddo})} = 5$). Animals were sacrificed, and the whole brains were dissected out within 20 s on an ice-cold surface. All tissue samples were pulverized in liquid nitrogen and stored at −80 °C for subsequent processing. Before killing, pregnant dams and offspring of both genotypes were weighted at different time points to analyze the potential effect of D-Asp depletion on body weight. We found no genotype effect or genotype × age interaction in both dams and offspring (dams: genotype, $F_{(1,12)} = 0.426$, $p = 0.5262$; genotype × age, $F_{(2,12)} = 0.925$, $p = 0.4232$; pups: genotype, $F_{(1,38)} = 2.104$, $p = 0.1551$; genotype × age, $F_{(4,38)} = 0.385$, $p = 0.8180$) (see Supporting Information Table S1).

NMR Sample Preparation

Brain samples were collected from mice according to the standard operating procedure for metabolomic-brain samples.[26,27] To each 15−30 mg sample of lyophilized tissue, 0.45 mL of water and 2 mL of methanol were added. The samples were then sonicated and diluted in a mixed solution of chloroform/water (2/1 mL), vortexed, and centrifuged at 10,000*g* for 10 min at 4 °C. After centrifugation, polar and apolar phases were separated and lyophilized (for details, see Supporting Information).[27] Polar phase was used for NMR analysis, while the apolar phase for HRMS analysis.

Dried polar extracts were dissolved into 500 μL of buffer (50 mM Na_2HPO_4, 1 mM trimethylsilyl propionic-2,2,3,3-d_4 acid, sodium salt (TSP-d_4), 50 μL of D_2O) and transferred into 5 mm NMR tubes for ^1H NMR detection. TSP-d_4 at 0.1% in D_2O was used as an internal reference for the alignment and quantification of NMR signals.[26,27]

NMR Spectra Acquisition

NMR experiments were acquired on a Bruker-AVANCE II 600 MHz spectrometer equipped with a 5 mm triple-resonance *z*-gradient CryoProbe (Bruker Co, Rheinstetten, Germany) at 310 K. Topspin, version 3.0, was used for spectrometer control and data processing (Bruker Biospin). 1D nuclear Overhauser enhancement spectroscopy (NOESY) experiments were acquired using a spectral width of 14 ppm, 16k data points, excitation sculpting for water suppression,[28] 192 transients, 4 s relaxation delay, and 60 ms mixing time. A weighted Fourier transform was applied to the time domain data with a 0.5 Hz line-broadening followed by manual phase and baseline correction in preparation for targeted profiling analysis.

NMR Data Analysis

Analysis of the NMR spectra was performed according to a targeted metabolomic approach. Specifically, the identity of the metabolites was established before statistical data analysis using Chenomx NMR-Suite v8.0 (Chenomx Inc., Edmonton, 252 Canada). ChenomxNMRSuite allows for the identification of the metabolites combining advanced analysis tools with a compound library. The signals within the selected spectral regions are identified for comparison with a database, including the NMR spectra of biological fluids and tissue extracts.

Quantitative analysis of NMR spectra was performed using NMRProcFlow.[29] The 1D NMR spectra were subjected to baseline correction, ppm calibration, spectral alignment, solvent suppression, and normalization by probabilistic quotient. After the processing, metabolites were quantified by choosing ppm ranges for each metabolite peak located in uncrowded areas of the spectrum to avoid contamination by adjacent ones. All the data needed for the quantification were exported into a spreadsheet workbook using the "qHNMR" template. The latter aggregates information within five separate tabs: the sample table, the bucket table, the signal-to-noise ratio matrix, and the values of integration for each bucket (columns) and each spectrum (rows). The workbook allows to include the data necessary for a correct quantification, such as sample volume (mL), the mg of brain tissue, the number of

https://dx.doi.org/10.1021/acs.jproteome.0c00622
J. Proteome Res. 2021, 20, 727−739

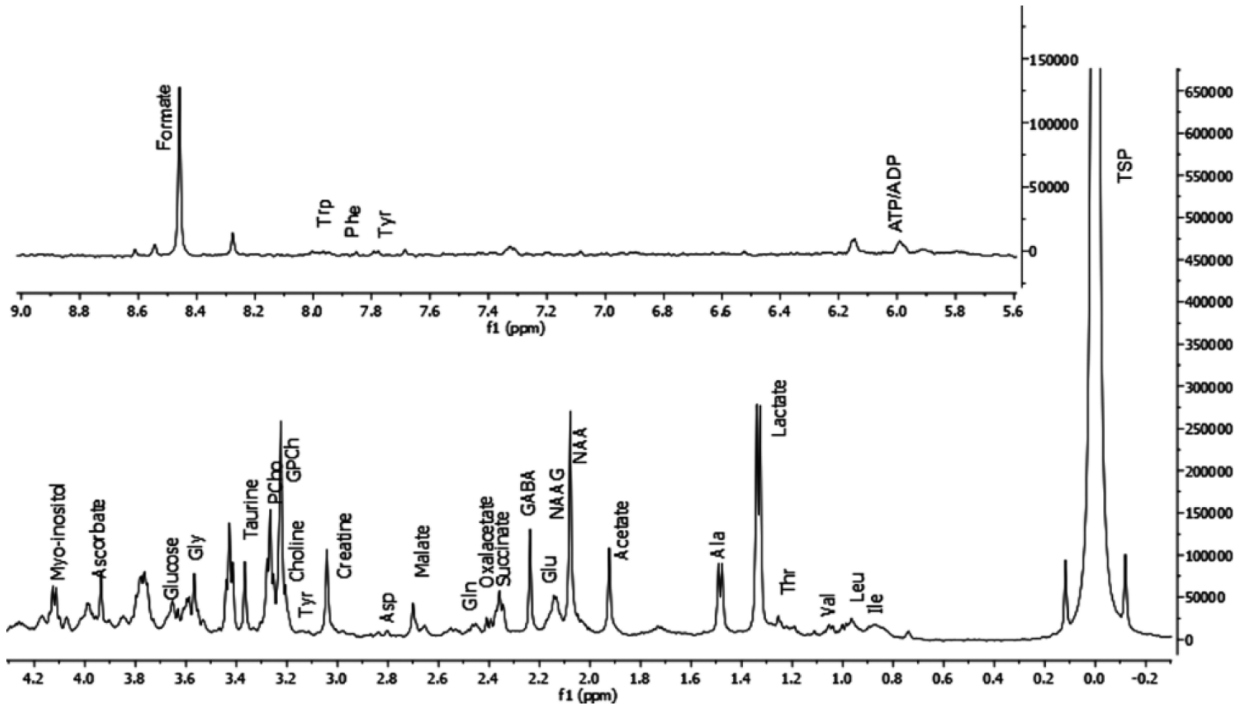

Figure 1. Representative 1D NOESY spectrum of mouse brain extracts (E13.5). The region on top is multiplied for better visualization. The spectrum is acquired at 600 MHz and T = 310 K. Thirty-one brain metabolites are identified and annotated.

protons related to the metabolites' peaks, and the molecular weight of the metabolites. The data matrix generated by NMRProcFlow was finally used for statistical analysis.

HRMS Sample Preparation and Processing

The nonpolar fraction was diluted in 200 μL of 1:1 MeOH 10 mM $HCOONH_4/CHCl_3$, centrifuged, and directly employed for direct infusion. Data were acquired on a SolariX XR 7T FT-ICR (Bruker Daltonics, Bremen, Germany) in direct infusion mode using a 250 μL Hamilton syringe at a flow rate of 2 μL/min. The instrument was tuned with a standard solution of sodium trifluoroacetate. Mass spectra were recorded in a broadband mode in the range 100−1500 m/z with an ion accumulation of 20 ms, 32 scans using two million data points (2 M), and a mass resolution of 200.000 at m/z 400. Nebulizing (N_2) and drying gases (air) were set at 1 and 4 mL/min, respectively, with a drying gas temperature of 200 °C. Both positive and negative ESI ionization were employed in separate runs. Funnel amplitude was set to 100 V, transfer optics: frequency 6 MHz, and time of flight 0.7 s. The instrument was controlled by Bruker FTMS Control. HRMS data set was published on the Massive platform with doi: 10.25345/C5PJ4R.

HRMS data analysis was performed with Metaboscape 4.0 (Bruker), where the first step is the creation of a feature matrix (bucket table) using the T-ReX 2D algorithm. Assignment of the molecular formula was performed for the detected features using SmartFormula (SF), isotopic fine structure (ISF) and data recalibration. The bucket table was annotated with a list of lipids obtained from the LIPIDMAPS database (www.lipidmaps.org). Annotation was performed with 0.2 ppm (narrow) or 0.5 ppm (wide) mass tolerance. Five replicates of each injection were performed.

Lipid metabolites detected by HRMS were putatively annotated with high accurate mass/ISF, level 2 of metabolomic standard initiative,[30,31] taking benefit of the ultra-high resolution, high mass accuracy, and ISF delivered by FT-ICR measurements.[32]

Statistical Analysis

Multivariate statistical analysis (MVA) and partial least-squares discriminant analysis (PLS-DA) were conducted with normalized metabolomics data using MetaboAnalyst 4.0 (http://www.metaboanalyst.ca/).[33] NMR data matrices were normalized by sum and Pareto scaling; moreover, HRMS data matrices were normalized by median and range scaling.

Two separated multivariate analyses have been conducted on the NMR and MS data set. The performance of the PLS-DA model was evaluated using the coefficient Q2 (using the 7-fold internal cross-validation method) and the coefficient R2, defining the variance predicted and explained by the model, respectively (see Supporting Information Table S2a,b). The loading plot was used to identify significant metabolites responsible for maximum separation in the PLS-DA score plot, and these metabolites were ranked according to their variable influence on projection (VIP) scores. VIP scores are weighted sums of the PLS-DA weights' squares, which indicate the importance of the variable.

RESULTS

Multivariate Data Analysis of NMR Data

Matrices, including metabolites and their concentrations derived from ^{1}H NMR data collected in 1D NOESY,[34,35] were analyzed according to MVA using MetaboAnalyst 4.0.[36] We prepared five matrices, including the samples for each developmental phase (E13.5 $R26_{(5)}^{+/+}$ *vs* $R26_{(5)}^{Ddo/Ddo}$; E16.5 $R26_{(5)}^{+/+}$ *vs* $R26_{(5)}^{Ddo/Ddo}$; E18.5 $R26_{(5)}^{+/+}$ *vs* $R26_{(5)}^{Ddo/Ddo}$; P3 $R26_{(4)}^{+/+}$ *vs* $R26_{(4)}^{Ddo/Ddo}$; and P7 $R26_{(5)}^{+/+}$ *vs* $R26_{(5)}^{Ddo/Ddo}$) and the metabolite concentrations. For each sample, 31 metabolites were identified and quantified. A representative ^{1}H NMR

https://dx.doi.org/10.1021/acs.jproteome.0c00622
J. Proteome Res. 2021, 20, 727−739

spectrum of polar extracts of whole brains is shown in Figure 1 with the metabolite signals indicated.

After normalization by sum and Pareto scaling, the data matrices were analyzed by univariate methods (fold change and T-test) (see Supporting Information Tables S3 and S4) and a multivariate supervised method, PLS-DA.[36] In Figure 2, PLS-DA shows that the data sets relative to the extracts of control $R26^{+/+}$ whole mouse brains are well separated from the extracts of mutant $R26^{Ddo/Ddo}$ whole mouse brains at each development phase. Table 1 reports the components with relative variances for the samples of each developmental phase.

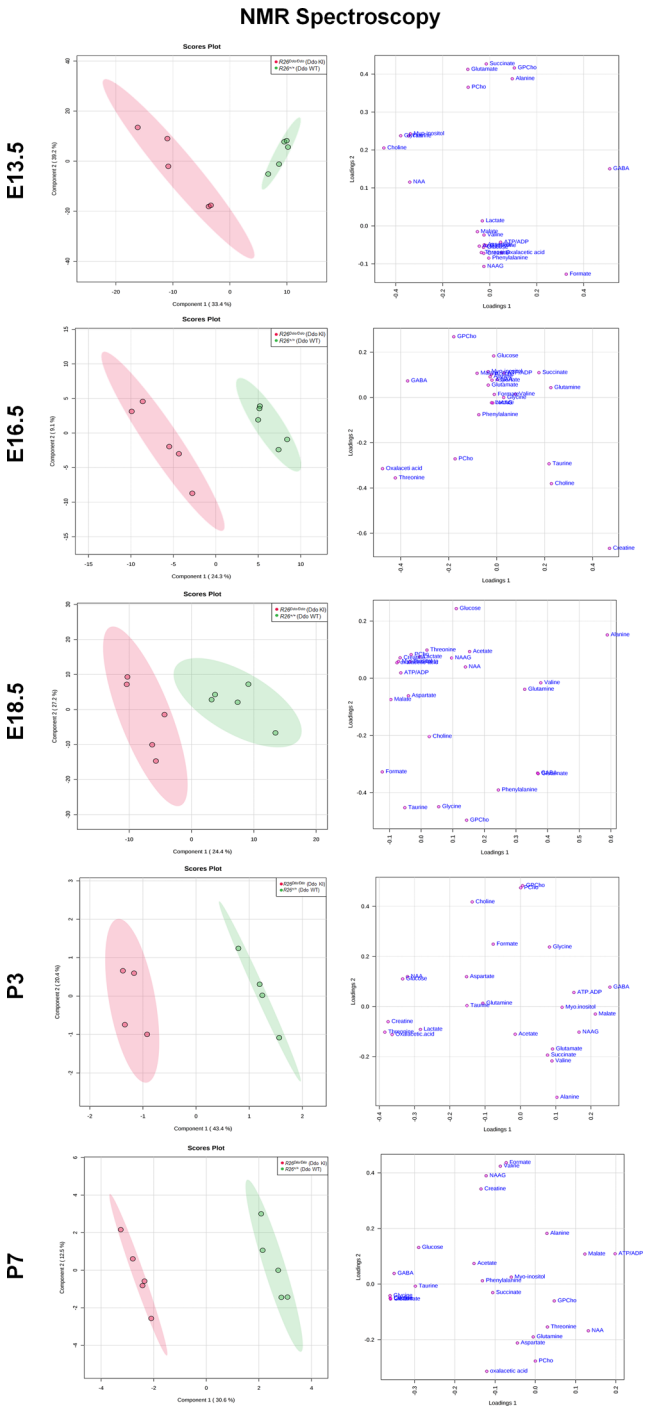

Figure 2. PLS-DA score scatter plot and PLS-DA loading scatter plot for the ^{1}H NMR data collected in 1D NOESY spectra acquired at 600 MHz. Data are relative to brain extracts of $R26^{+/+}$ (green circles) and $R26^{Ddo/Ddo}$ (red circles) mice for each development phase: E13.5 (5), E16.5 (5), E18.5 (5), P3 (4), and P7 (5).

Table 1. Percentage Variance of Components Relative to the Sample of Each Developmental Phase

phase	1° component (%)	2° component (%)
E13.5	33.4	39.2
E16.5	24.3	9.1
E18.5	24.4	27.2
P3	43.4	20.4
P7	30.6	12.5

Inspection of the PLS-DA score scatter plots and loading scatter plots (Figure 2) shows that several metabolites significantly discriminate polar extracts of control $R26^{+/+}$ whole mouse brains from polar extracts of mutant $R26^{Ddo/Ddo}$ whole mouse brains. This evidence is confirmed by applying VIP score analysis (Figure 3). Accordingly, the metabolites characterized by a VIP score higher than one are considered good classifiers between the two genotypes in each phase.

The Cartesian space of representation is described by the presence of the most discriminating metabolites between the two genotypes, according to the value of the VIP score. As reported in the VIP graph, $R26^{Ddo/Ddo}$ mutant brains at the E13.5 embryonal phase are different from the relative $R26^{+/+}$ control mouse brains because they are characterized by changes in the concentration of γ-aminobutyric acid (GABA), choline, glycine, L-alanine, and *N*-acetyl-aspartate (NAA). Moreover, we identified different L-threonine, creatine, GABA, and L-glutamine concentrations in $R26^{Ddo/Ddo}$ mutant brains at E16.5 compared to $R26^{+/+}$ control mouse brains. At E18.5, we detected changes in L-alanine, L-glutamine, L-glutamate, GABA, and L-valine. VIP metabolic analysis recognized a different metabolic profile also in early postnatal tissues. In detail, in P3 $R26^{Ddo/Ddo}$ mutants, we found variations related to L-threonine, creatine, glucose, and NAA, while in P7 $R26^{Ddo/Ddo}$ mutants, we found variations related to choline, lactate, L-glutamate, glycine, and GABA. Importantly, in line with the deaminative oxidation catalyzed by DDO, which produces oxaloacetic acid from D-Asp,[9,10] and consistent with the striking increased DDO activity observed in *Ddo* knockin mice,[4] we found that this ketoacid appears to be the most discriminating metabolite at E16.5 and P3, as its concentration increases in $R26^{Ddo/Ddo}$ mice compared to controls.

Multivariate Data Analysis of HRMS Data

Data acquired using mass spectrometry define a lipidomic matrix that includes the average of the intensities, derived from the five measurements for each sample's detected features. As reported in Table S5 of Supporting Information, after alignment and filtering, 120 lipids were annotated for each sample for each brain developmental phase. The data, after normalization by median and range scaling, were analyzed by the univariate analysis made by T-test and fold change (see Supporting Information Table S5)[36] and the multivariate supervised method, PLS-DA (MetaboAnalyst 4.0).[36]

Figure 4 shows the PLS-DA for the data sets exhibiting a characteristic lipidomic profile in $R26^{+/+}$ compared to $R26^{Ddo/Ddo}$. In particular, the lipidomic profile of $R26^{Ddo/Ddo}$ mouse brains at the E13.5 and P7 development phases is significantly different than the lipidomic profile of $R26^{+/+}$. At

https://dx.doi.org/10.1021/acs.jproteome.0c00622
J. Proteome Res. 2021, 20, 727−739

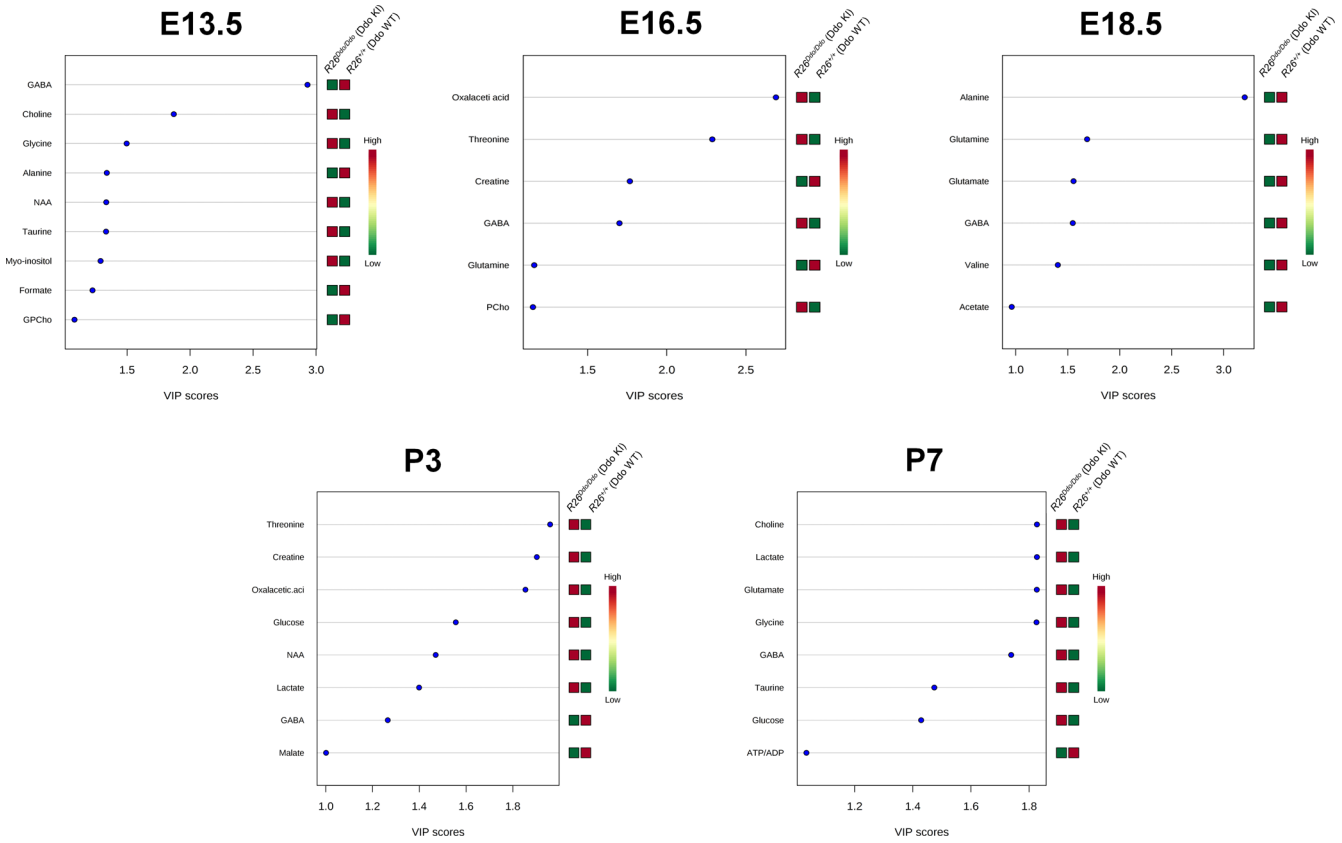

Figure 3. Metabolites discriminating $R26^{+/+}$ from $R26^{Ddo/Ddo}$ based on NMR-based metabolomic analysis of whole-brain polar extracts at different embryonal and postnatal development stages.

the E13.5 brain developmental phase, the first component explains 32% of the variance, while the second explains 17.7%; at the P7 developmental phase, the first component explains 18.7% of the variance, while the second explains 13.4%.

An examination of the PLS-DA score scatter plots and loading scatter plots (Figure 4) points to different metabolites that significantly discriminate apolar extracts of $R26^{Ddo/Ddo}$ mouse brains from $R26^{+/+}$ mouse brains. This evidence is confirmed by applying VIP score analysis (Figure 5). The graphs reported in Figure 5 show that apolar extracts of $R26^{Ddo/Ddo}$ mouse brains at E13.5 are characterized by variations of several lipid classes, in particular long chain fatty acid derivatives (palmitoylcarnitine), phosphocholines (PC(33:2), PC(38:5), and PC(35:4)), phosphoserines (PS(O-33:1)) and sphingomyelines (SM(d18:1/18:0)) (see Supporting Information Table S6). Moreover, apolar extracts of $R26^{Ddo/Ddo}$ mouse brains at P7 are characterized by changes in phosphocholines (PC(40:6), PC(32:2) and PC(36:5)), phosphoserines (PS(O-33:1)), and sphingolipids (Cer(d18:1/18:0) and SM(d18:1/18:0)) (see Supporting Information Table S7 and Figure S1).

Combined Pathway Analysis

To analyze the previously reported data, we applied metabolic pathway analysis using MetaboAnalyst 4.0 and Reactome[37] software. Pathway analysis included both ^{1}H NMR and HRMS data. Data reported in Tables 2 and 3 indicate all matched pathways according to *p*-values and false discovery rate (FDR) values. The pathways were classified according to the total number of compounds found in the KEGG database.[38,39] The pathway impact is correlated with the number of metabolites involved (number of hits). By combining pathways characterized by hits >1 and *p*-values < 0.05, we observed the pathways most perturbed in our analysis in each development phase.

Pathway analysis was further optimized by Reactome.[37] The function analysis tool was used to identify the pathways featuring the different brain development phases more accurately. All Reactome pathways are shown in Tables 2 and 3, classified according to the *p*-value and FDR values. Interestingly, the analysis of metabolic pathways made by MetaboAnalyst and Reactome identifies a potential relationship between aspartate metabolism and the macro areas of solute-carrier gene (SLC) disease.

OmicsNet Analysis

The metabolite data have been uploaded in PubChem entry format into the OmicsNet platform of MetaboAnalyst 4.0, a platform for multiomics analysis. As a result, we qualitatively assessed the relationship between the NMR and HRMS metabolites. Furthermore, thanks to the multi-omic vision of OmicsNet, the possible genes related to these metabolites and their networks are identified.

Figure 6 shows the modules derived by OmicsNet. The modules refer to parts of networks that have higher connections than the average connections expected over the whole network. Networks were displayed using Waltrap, Label Propagation, and InfoMap algorithms.[40,41] All the modules were classified by size and *p*-value. Figure 6 shows that the aspartate pathway, with a *p*-value of 2.41×10^{-21}, is the most significant (*p*-value <0.05 calculated by T-test). The genomics analysis of this pathway shows a link with several genes correlated to cognitive disabilities, schizophrenia, and brain

https://dx.doi.org/10.1021/acs.jproteome.0c00622
J. Proteome Res. 2021, 20, 727−739

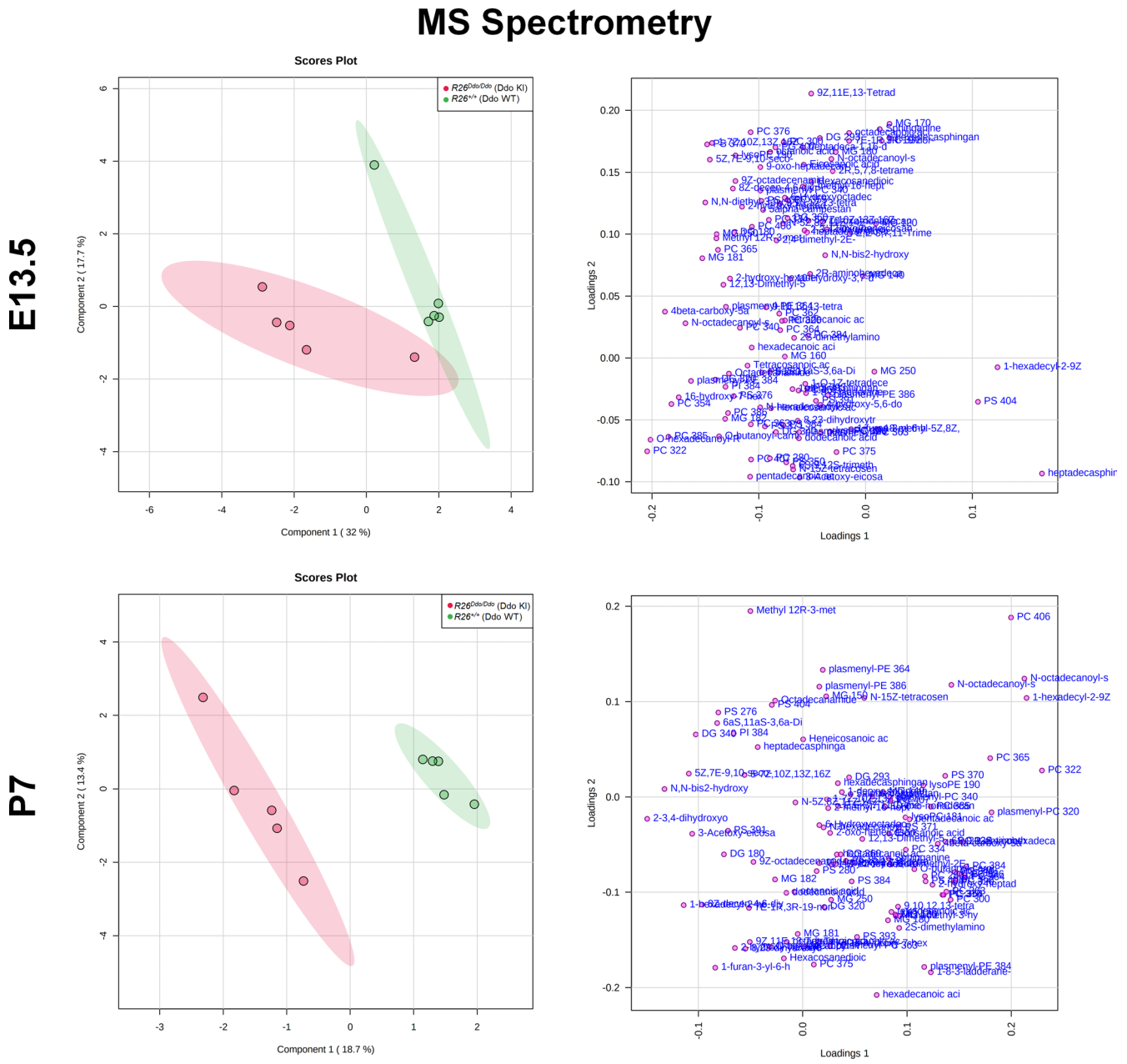

Figure 4. PLS-DA score scatter plot and PLS-DA loading scatter plot for the HRMS data acquired on a SolariX XR 7T. Data are relative to brain extracts of $R26^{+/+}$ mice (green circles) and $R26^{Ddo/Ddo}$ mice (red circles) for development phases E13.5 (5) and P7 (5).

aging and therefore with possible SLC disorder, as shown by Reactome.

DISCUSSION

The concentration of D-Asp in the brain follows a specific temporal occurrence, being much higher during the embryonic stage compared to postnatal life.[1−5] This time-dependent change is due to the *Ddo* gene expression and the consequent activity of DDO enzyme in the postnatal period.[1,42] Although the spatiotemporal distribution of D-Asp in the brain has been extensively investigated, its physiological role in the developmental brain is still largely unknown.

To determine the metabolic influence played by D-Asp in the developing brain, in this study, we characterized the metabolomic fingerprint of embryonic and early postnatal $R26^{Ddo/Ddo}$ brains, compared to $R26^{+/+}$controls. To this end, ^{1}H NMR spectroscopy and HRMS techniques were used to analyze brain extracts of $R26^{+/+}$and $R26^{Ddo/Ddo}$ mice. NMR spectroscopy and HRMS are the techniques of choice to define the metabolic profile of biofluids and tissue extracts; they are complementary analytical techniques and often used in parallel.

MVA of data obtained from polar extracts by ^{1}H NMR spectroscopy indicated that characteristic metabolomic fingerprints distinguish $R26^{Ddo/Ddo}$ from $R26^{+/+}$ brains in both embryonic and postnatal stages. We found that cerebral D-Asp depletion increased choline, glycine, NAA, taurine, oxaloacetate, L-threonine, glucose, and lactate. All these molecules were upregulated at one prenatal and one postnatal time-point, except glucose and lactate, which were increased at postnatal but not prenatal phases (both P3 and P7). Myo-inositol and PCho increased at only one time-point, E13.5 and E16.5, respectively. On the other hand, D-Asp depletion is

https://dx.doi.org/10.1021/acs.jproteome.0c00622
J. Proteome Res. 2021, 20, 727−739

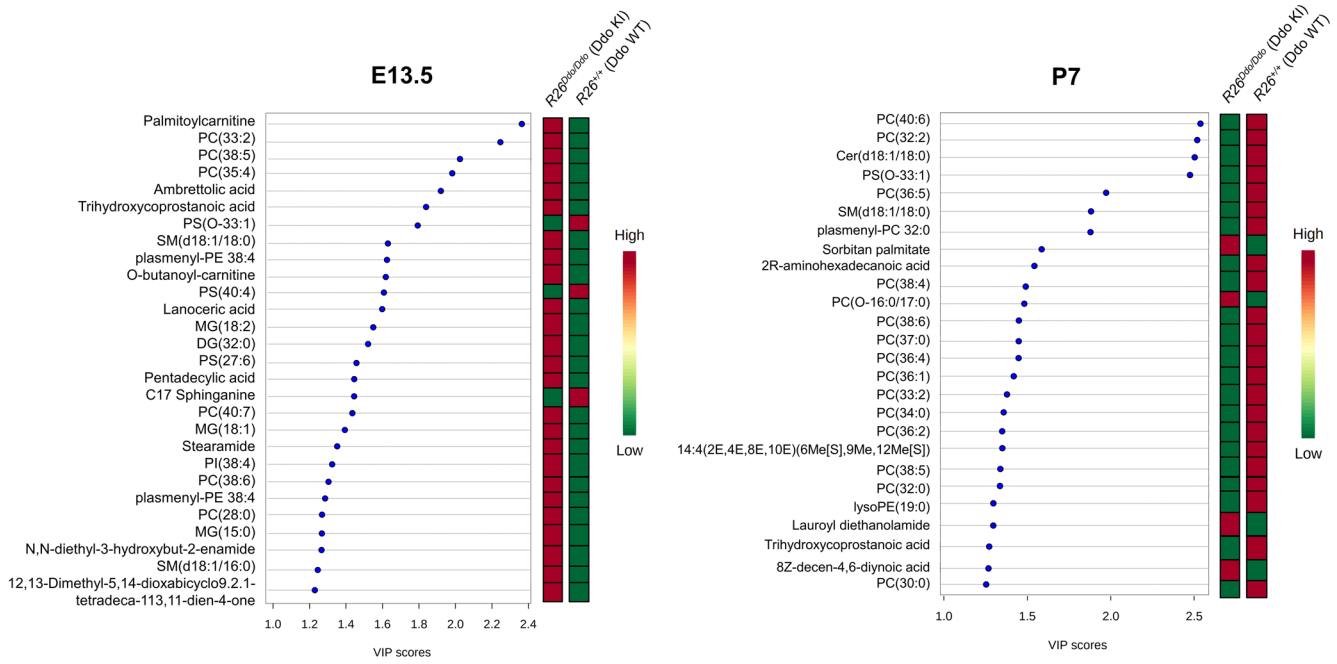

Figure 5. VIP score analysis: metabolites discriminating mouse brain apolar extracts of $R26^{+/+}$ from $R26^{Ddo/Ddo}$ at the E13.5 and P7 brain development phases.

Table 2. Metabolic Pathways Potentially Related to Each Embryonal Phase of Mice According to *p*-Values and FDR Values

		E13.5		E16.5		E18.5	
pathway name	pathway source	*p*-value	FDR	*p*-value	FDR	*p*-value	FDR
arginine and proline metabolism	MetaboAnalyst	9.97×10^{-7}	3.59×10^{-5}				
alanine, aspartate and glutamate metabolism	MetaboAnalyst	1.70×10^{-2}	2.64×10^{-1}	3.24×10^{-3}	1.17×10^{-2}	2.53×10^{-3}	2.28×10^{-2}
glycine, serine and threonine metabolism	MetaboAnalyst	4.36×10^{-2}	3.60×10^{-1}				
glycerophospholipid metabolism	MetaboAnalyst	5.00×10^{-2}	3.60×10^{-1}				
sphingolipid metabolism	MetaboAnalyst	1.12×10^{-2}	8.25×10^{-1}				
biosynthesis of unsaturated fatty acids	MetaboAnalyst	3.16×10^{-2}	8.25×10^{-1}				
linoleic acid metabolism	MetaboAnalyst	3.93×10^{-2}	8.25×10^{-1}				
fatty acid degradation	MetaboAnalyst	3.66×10^{-2}	8.25×10^{-1}				
glycolysis−gluconeogenesis	MetaboAnalyst			6.62×10^{-8}	1.31×10^{-6}	1.17×10^{-4}	3.80×10^{-3}
pyruvate metabolism	MetaboAnalyst			7.28×10^{-8}	1.31×10^{-6}	2.30×10^{-3}	2.28×10^{-2}
glyoxylate and dicarboxylate metabolism	MetaboAnalyst			2.77×10^{-7}	3.02×10^{-6}		
D-glutamine and D-glutamate metabolism	MetaboAnalyst			5.11×10^{-5}	2.71×10^{-4}		
arginine biosynthesis	MetaboAnalyst			5.27×10^{-5}	2.71×10^{-4}		
aminoacyl-tRNA biosynthesis	MetaboAnalyst					8.18×10^{-3}	5.89×10^{-2}
defective SLC6A19 causes Hartnup disorder (HND)	Reactome	1.93×10^{-5}	0.008	4.69×10^{-6}	0.002	2.32×10^{-5}	0.011
aspartate and asparagine metabolism	Reactome	2.38×10^{-5}	0.008	6.26×10^{-6}	0.002	3.10×10^{-5}	0.011
Na^+/Cl^- dependent neurotransmitter transporters	Reactome	2.39×10^{-4}	0.067	5.01×10^{-5}	0.012	3.08×10^{-4}	0.083
degradation of GABA	Reactome	4.18×10^{-4}	0.084	1.81×10^{-4}	0.031	4.80×10^{-4}	0.095
defective SLC1A1 is implicated in schizophrenia 18 (SCZD18) and dicarboxylic aminoaciduria	Reactome	0.003	0.173			0.003	0.189
defective GSS causes glutathione synthetase deficiency	Reactome			8.06×10^{-4}	0.069	0.002	0.16

associated with reduced malate, L-valine, acetate, L-alanine, formate, GPCho, L-glutamine, and ATP/ADP levels, at least at one time-point analyzed. Of these metabolites, only malate and ATP/ADP were reduced postnatally (P3 and P7, respectively) (see Supporting Information Figures S2−S4).

VIP score analysis points to GABA and L-glutamate, as discriminating metabolites with fluctuating concentrations over the different time-points between genotypes. GABA is the primary inhibitory neurotransmitter required for the control of synaptic excitation. GABA and L-glutamate belong to a common metabolic pathway: GABA is synthesized for decarboxylation by glutamic acid decarboxylases (GADs).[43] Therefore, GABA and GADs concentrations have been found highly correlated and spatiotemporally regulated during the rat brain's postnatal development.[44] Our data confirm this evidence: indeed, GABA concentration patterns at different

https://dx.doi.org/10.1021/acs.jproteome.0c00622
J. Proteome Res. 2021, 20, 727−739

Table 3. Metabolic Pathways Potentially Related to Each Postnatal Phase of Mice According to *p*-Values and FDR Values

		P3		P7	
pathway name	pathway source	*p*-value	FDR	*p*-value	FDR
valine, leucine and isoleucine biosynthesis	MetaboAnalyst	2.39×10^{-7}	7.39×10^{-6}		
glycine, serine and threonine metabolism	MetaboAnalyst	1.26×10^{-6}	1.95×10^{-5}	1.05×10^{-7}	6.28×10^{-7}
arginine and proline metabolism	MetaboAnalyst	2.49×10^{-5}	2.58×10^{-4}	9.36×10^{-7}	3.37×10^{-6}
pyruvate metabolism	MetaboAnalyst	3.67×10^{-3}	2.84×10^{-2}		
alanine, aspartate and glutamate metabolism	MetaboAnalyst	2.04×10^{-2}	6.32×10^{-2}	1.07×10^{-4}	2.74×10^{-4}
glutathione metabolism	MetaboAnalyst			2.66×10^{-9}	4.80×10^{-8}
D-glutamine and D-glutamate metabolism	MetaboAnalyst			1.02×10^{-8}	9.17×10^{-8}
aminoacyl-tRNA biosynthesis	MetaboAnalyst			7.13×10^{-8}	5.13×10^{-7}
histidine metabolism	MetaboAnalyst			2.02×10^{-7}	1.04×10^{-6}
glycerophospholipid metabolism	MetaboAnalyst			2.71×10^{-7}	1.22×10^{-6}
arginine biosynthesis	MetaboAnalyst			3.53×10^{-7}	1.41×10^{-6}
glyoxylate and dicarboxylate	MetaboAnalyst			1.52×10^{-5}	4.57×10^{-5}
sphingolipid metabolism	MetaboAnalyst			1.81×10^{-3}	1.52×10^{-1}
glycerophospholipid metabolism	MetaboAnalyst			5.31×10^{-3}	2.23×10^{-1}
α-linolenic acid metabolism	MetaboAnalyst			4.25×10^{-2}	8.92×10^{-1}
defective SLC6A19 causes Hartnup disorder	Reactome	9.54×10^{-6}	0.003	1.24×10^{-5}	0.004
defective GCLC causes hemolytic anemia due to γ-glutamylcysteine synthetase deficiency	Reactome	9.95×10^{-4}	0.086	0.001	0.104
SLC transporter disorders	Reactome	0.002	0.106	0.003	0.155
defective SLC1A1 is implicated in schizophrenia 18 (SCZD18) and dicarboxylic aminoaciduria	Reactome	0.002	0.106	0.002	0.132

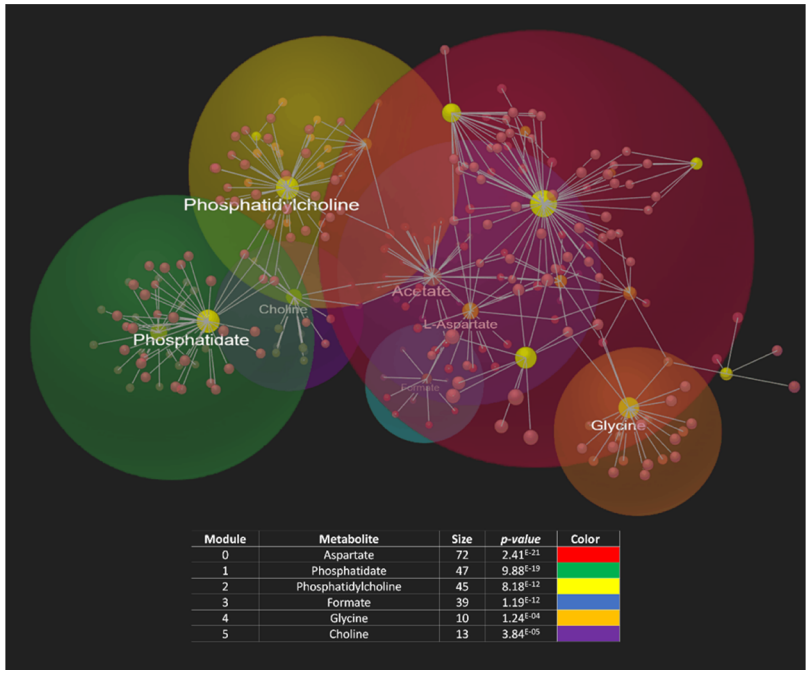

Figure 6. Graph Force module regarding the elaboration of the data matrix through OmicsNet. Each module (pathway) is labeled with different colors; the circles represent metabolites and genes involved in the pathway. The table describes the subnetworks searched by OmicsNet with their *p*-value and relative size (abundance of metabolites).

stages of embryonic and postnatal development are superimposable to those previously observed for GADs.[45] The nonlinear trajectory of GABA and L-glutamate concentrations can be interpreted in the frame of the critical function that GABA and GADs have shown to exert during early brain development as trophic factors for the regulation of proliferation and synapse formation.[46,47] These roles, although extensively investigated, remain almost undisclosed for their underlying mechanisms. Future studies may help understand possible crosslinking between *Ddo* and GAD expression, as increasing evidence shows that both are involved in the onset of pathologic conditions such as schizophrenia.[48]

Concerning other metabolites following unexpected concentration patterns, we cannot exclude that the analysis of whole-brain samples, rather than discrete brain subregions, could have produced net concentrations of differences between genotypes at different time-points. Future studies using a larger cohort of mutant mice and discrete brain subregions are mandatory to clarify this puzzling issue.

https://dx.doi.org/10.1021/acs.jproteome.0c00622
J. Proteome Res. 2021, 20, 727−739

Interestingly, a significant number of deregulated molecules are involved in neurotransmission. Indeed, among the increased metabolites, we found glycine, choline, and taurine. In addition to its role in proteinogenesis and cell metabolism, glycine is involved in regulating NMDA receptor signaling as an important coagonist at glutamatergic synapses.[49−51] Choline plays a central role in brain development because it is an essential brain precursor of the acetylcholine neurotransmitter.[52−55] Consistent with this finding, deficits in choline levels in the brain during gestation are known to cause alterations in cognitive functions.[52,55] In addition to choline, the VIP score also indicates a variation in other choline class compounds, such as GPCho and PCho.[56] Finally, taurine appears to act as a major inhibitory neurotransmitter/modulator in the embryonic and early postnatal brain, having much higher concentrations than GABA in most brain areas.[57] Interestingly, these three molecules increase at the same time-points (E13.5 and P7), indicating an overall change in neurotransmission in these phases (see Supporting Information Figure S4). Other significant D-Asp-mediated changes potentially affecting glutamatergic neurotransmission include GABA and L-glutamate, whose levels, as discussed above, fluctuate at the different periods analyzed. In particular, MVA identified the inhibitory neurotransmitter, GABA, as a discriminating metabolite between genotypes at all stages tested. Interestingly, our recent work has already shown a potential link between D-Asp and GABAergic neurotransmission because we found that D-Asp deprivation results in an increased number of cortical parvalbumin-positive GABAergic interneurons in adult $R26^{Ddo/Ddo}$ brains.[4] Therefore, based on these observations, future studies are required to understand the influence of early D-Asp in regulating cellular GABA levels and the potential causal relationship with the number of parvalbumin-positive GABAergic interneurons.

In line with the ability of D-Asp to influence glutamatergic neurotransmission, analysis of the brain polar extracts provided evidence that D-Asp depletion in mutants induces changes in the L-glutamate concentration at P7 in $R26^{Ddo/Ddo}$ compared to $R26^{+/+}$ mice. This observation is discrepant with that provided by HPLC methods, in which the levels of L-glutamate were unchanged between $R26^{Ddo/Ddo}$ and $R26^{+/+}$ brains.[4] In this regard, we cannot exclude the possibility that differences in method sensitivity might account for this discrepancy.

Remarkably, in agreement with the production of oxaloacetate by DDO,[9,10] and in line with an abnormally increased enzymatic DDO activity in $R26^{Ddo/Ddo}$,[4] the VIP score values of NMR data showed an increase in oxaloacetate concentrations at E16.5 and P3 in $R26^{Ddo/Ddo}$ brains compared to controls.

Furthermore, MVA allowed us to identify other dysmetabolism associated with D-Asp depletion and linked to L-amino acids, including L-threonine and L-valine. In particular, VIP score analysis showed an increment of L-threonine in E16.5 $R26^{Ddo/Ddo}$ and P3 $R26^{Ddo/Ddo}$ brains compared to controls. Threonine is a central amino acid because it has significant involvement in glycine and serine metabolism, as well as in choline and creatine, and valine, leucine, and isoleucine biosynthesis (see Supporting Information Figure S3).[58]

On the other hand, we reported lower L-alanine and L-valine concentrations in the brain of $R26^{Ddo/Ddo}$ mice at E18.5 compared to controls.

Overall, our NMR and HRMS data in *Ddo* knockin brains suggest, for the first time, a prominent influence for prenatal and early postnatal D-Asp occurrence in modulating the metabolism of L-amino acids, such as L-alanine, L-valine, L-serine, and L-threonine, as well as of glycine.

A further observation obtained by MVA is the alteration of creatine concentrations in $R26^{Ddo/Ddo}$ brains at E16.5 and P3, compared to controls. Although the meaning of its altered concentration in the mutant brain remains unclear, it is relevant to remark that creatine is essential for proper brain development, and its reduction causes severe neuronal malfunctions.[54,59−61]

NMR analysis allowed us to identify considerable alterations in the brain energy metabolism of $R26^{Ddo/Ddo}$ mouse brains. The mechanisms of lipid synthesis and energy production in the brain are very peculiar. Numerous metabolites participate in brain lipid metabolism, including NAA, which is synthesized from L-aspartate and acetyl-coenzyme A in neurons.[62−66] During postnatal central nervous system development, the expression of lipogenic enzymes, such as the NAA-degrading enzyme aspartoacylase (ASPA),[67] increase in oligodendrocytes along with the production of NAA in neurons.[62,68,69] Interestingly, our metabolomic analysis showed evidence that the lack of D-Asp is linked to an increment of NAA in $R26^{Ddo/Ddo}$ mouse tissues at E13.5 and P3 compared to $R26^{+/+}$ mice. Besides lipids, other metabolites involved in brain energetic processes have been identified by VIP analysis in $R26^{Ddo/Ddo}$ brain tissues, such as oxaloacetate, glucose, lactate, and malate, directly involved in the Krebs cycle (see Supporting Information Figure S2).

We have previously shown a relationship between dysfunctional cerebral D-Asp metabolism and schizophrenia.[23,24,70] Interestingly, analysis of the pathways carried out by Reactome[37] in $R26^{Ddo/Ddo}$ mutant brains provided supporting evidence relative to the dysmetabolism of the SLC transporters and, in particular, of defective SLC1A1 pathway in psychiatric disorders, including schizophrenia (Table 3).[71−73]

Moreover, in $R26^{Ddo/Ddo}$ mutant brains, other altered pathways have been identified by OmicsNet[41] (Figure 6). In particular, the aspartate pathway revealed a connection with the presence of the glycine amidinotransferase mitochondrial gene, whose mutation causes a congenital error of creatine synthesis characterized by cognitive impairment, language impairment, and behavior disorders.[74−76]

Although the overall findings obtained in $R26^{Ddo/Ddo}$ mice indicate an involvement of D-Asp depletion in the brain's fundamental metabolic processes, some intrinsic limitations of this work should also be discussed to target future studies and determine the next objectives. First, our biochemical studies have been performed on total brain homogenates. Therefore, it is mandatory to perform further metabolomic analyses on brain homogenates and microdialysis samples to evaluate whether these alterations are found in the extracellular space where these molecules directly influence neurotransmission. Moreover, it will be of fundamental importance to focus future studies on specific brain regions to understand if the deregulations observed in this study are region-specific or are part of more massive changes affecting larger brain regions or the whole brain. In both cases, it is essential to evaluate whether cerebral changes in energy and amino acid metabolism are influenced, at least in part, by peripheral alterations because all the deregulated molecules we found also take part in peripheral metabolic processes. In this regard, molecules such as L-glutamate, glycine, GABA, and taurine are

https://dx.doi.org/10.1021/acs.jproteome.0c00622
J. Proteome Res. 2021, 20, 727−739

neurotransmitters and important cellular metabolites regulating different intracellular metabolic pathways.

Another critical point is related to clarify whether the metabolomic changes observed in this study are also extended to adulthood. Because D-Asp levels are the highest during the developmental phase,[1−5] the early time points we chose for our analyses are those at which there is the widest gap in D-Asp levels between *Ddo* knockin and wild-type mice. Therefore, it is useful to evaluate whether the metabolomic alterations found in this work in the prenatal and early postnatal phases are also extended at adulthood when cerebral D-Asp levels strongly decrease. Finally, future investigations will be addressed to understand the biochemical relationship between D-Asp and the deregulated molecules found in this study because none of them, except oxaloacetate, directly links with D-Asp metabolism. In this regard, future studies will also help assess the expression levels and the activity of the main enzymes involved in these molecules' homeostasis.

CONCLUSIONS

Our metabolomic analysis conducted on polar and apolar extracts using ^{1}H NMR and HRMS, respectively, has helped to elucidate the role of D-Asp as a signaling molecule involved in neural metabolism. The overexpression of the DDO enzyme and the consequent D-Asp depletion during prenatal and early postnatal development affect various metabolic L-amino acid pathways such as L-threonine, L-glycine, L-alanine, L-valine, and L-glutamate. Furthermore, we found variations of metabolites involved in brain development and functions (choline, creatine, PCho, GPCho, sphingolipids, and glycerophospholipids) and in brain energy metabolism (GPCho, glucose, and lactate). These results suggest that early cerebral D-Asp and its degradation by DDO might regulate intracellular metabolic pathways so far never evaluated, thus extending the influence of this D-amino acid beyond its well-known role in neurotransmission.

ASSOCIATED CONTENT

Supporting Information

The Supporting Information is available free of charge at https://pubs.acs.org/doi/10.1021/acs.jproteome.0c00622.

Sum average intensity related to the most important lipid classes detected by HRMS; comparison of mean concentrations of the most significant metabolites related to brain energetic metabolism at various stages of brain development; comparison of mean concentrations of the most significant metabolites related to amino acid metabolism at various stages of brain development; comparison of mean concentrations of the most significant metabolites related to metabolism of neurotransmitters at various stages of brain development; body weight of $R26^{+/+}$ and $R26^{Ddo/Ddo}$ pups and pregnant dams during prenatal and postnatal development; PLS-DA classification of the five different components (comps) based on accuracy; important features identified by fold change and logarithmic fold change [log 2(FC)] parameters calculated; important features identified by T-test values, *p*-values (threshold < 0.05), logarithmic *p*-values, and FDR parameters calculated for the most statistically significant compounds; identified lipids from apolar extracts of whole brains; VIP score relate to identified lipids in all brains at E13.5; and VIP score related to identified lipids in all brains at P7 (PDF)

AUTHOR INFORMATION

Corresponding Authors

Alessandro Usiello − *Laboratory of Behavioural Neuroscience, Ceinge Biotecnologie Avanzate, 80145 Naples, Italy; Department of Environmental, Biological and Pharmaceutical Science and Technologies (DISTABIF), University of Campania, L. Vanvitelli, 81100 Caserta, Italy*; Email: usiello@ceinge.unina.it

Anna Maria D'Ursi − *Department of Pharmacy, University of Salerno, 132-84084 Fisciano, Salerno, Italy*; orcid.org/0000-0001-6814-8472; Phone: +39089969748; Email: dursi@unisa.it

Authors

Manuela Grimaldi − *Department of Pharmacy, University of Salerno, 132-84084 Fisciano, Salerno, Italy*; orcid.org/0000-0001-7354-8008

Carmen Marino − *Department of Pharmacy and PhD Program in Drug Discovery and Development, University of Salerno, 132-84084 Fisciano, Salerno, Italy*

Michela Buonocore − *Department of Pharmacy and PhD Program in Drug Discovery and Development, University of Salerno, 132-84084 Fisciano, Salerno, Italy*; orcid.org/0000-0003-1189-1729

Angelo Santoro − *Department of Pharmacy and PhD Program in Drug Discovery and Development, University of Salerno, 132-84084 Fisciano, Salerno, Italy*; orcid.org/0000-0002-9690-907X

Eduardo Sommella − *Department of Pharmacy, University of Salerno, 132-84084 Fisciano, Salerno, Italy*

Fabrizio Merciai − *Department of Pharmacy and PhD Program in Drug Discovery and Development, University of Salerno, 132-84084 Fisciano, Salerno, Italy*

Emanuela Salviati − *Department of Pharmacy and PhD Program in Drug Discovery and Development, University of Salerno, 132-84084 Fisciano, Salerno, Italy*

Arianna De Rosa − *Laboratory of Behavioural Neuroscience, Ceinge Biotecnologie Avanzate, 80145 Naples, Italy; Department of Environmental, Biological and Pharmaceutical Science and Technologies (DISTABIF), University of Campania, L. Vanvitelli, 81100 Caserta, Italy*

Tommaso Nuzzo − *Laboratory of Behavioural Neuroscience, Ceinge Biotecnologie Avanzate, 80145 Naples, Italy; Department of Environmental, Biological and Pharmaceutical Science and Technologies (DISTABIF), University of Campania, L. Vanvitelli, 81100 Caserta, Italy*

Francesco Errico − *Department of Agricultural Sciences, University of Naples "Federico II", 100-80055 Portici, Italy*

Pietro Campiglia − *Department of Pharmacy, University of Salerno, 132-84084 Fisciano, Salerno, Italy; European Biomedical Research Institute of Salerno, 84125 Salerno, Italy*; orcid.org/0000-0002-1069-2181

Complete contact information is available at: https://pubs.acs.org/10.1021/acs.jproteome.0c00622

Author Contributions

M.G. and C.M. contributed equally to this study. M.G. prepared the NMR samples and acquired and analyzed the NMR spectra, C.M. performed the statistical analysis, M.B. and

https://dx.doi.org/10.1021/acs.jproteome.0c00622
J. Proteome Res. 2021, 20, 727−739

A.S. analyzed the NMR spectra, Eduardo Sommella prepared the HRMS samples, F.M. acquired the FT-ICR data, Emanuela Salviati acquired and analyzed the HRMS data, A.D.R. and T.N. collected the brain tissues, P.C. supervised the HRMS analysis, F.E. wrote the manuscript, and A.U. and A.M.D. conceived the work and composed the manuscript.

Notes

The authors declare no competing financial interest.

■ ACKNOWLEDGMENTS

A.U. was supported by a grant from MIUR (Ministero dell'Istruzione, dell'Università e della Ricerca, Progetto PRIN 2017-Project nr 2017M42834).

■ ABBREVIATIONS

Ddo, D-aspartate oxidase; PCho, phosphocholine; GPCho, glycerophosphocholine; NMDA, *N*-methyl D-aspartate; NAA, *N*-acetyl-aspartate; NAAG, *N*-acetylaspartylglutamic acid; NMR, nuclear magnetic resonance; HRMS, high-resolution mass spectrometry; PLS-DA, partial least-squares discriminant analysis; VIP, variable influence on projection; FDR, false discovery rate; SLC, solute-carrier gene; MVA, multivariate statistical analysis

■ REFERENCES

(1) Punzo, D.; Errico, F.; Cristino, L.; Sacchi, S.; Keller, S.; Belardo, C.; Luongo, L.; Nuzzo, T.; Imperatore, R.; Florio, E.; De Novellis, V.; Affinito, O.; Migliarini, S.; Maddaloni, G.; Sisalli, M. J.; Pasqualetti, M.; Pollegioni, L.; Maione, S.; Chiariotti, L.; Usiello, A. Age-related changes in D-aspartate oxidase promoter methylation control extracellular D-aspartate levels and prevent precocious cell death during brain aging. *J. Neurosci.* **2016**, *36*, 3064−3078.

(2) Hashimoto, A.; Kumashiro, S.; Nishikawa, T.; Oka, T.; Takahashi, K.; Mito, T.; Takashima, S.; Doi, N.; Mizutani, Y.; Yamazaki, T.; et al. Embryonic development and postnatal changes in free D-aspartate and D-serine in the human prefrontal cortex. *J. Neurochem.* **1993**, *61*, 348−351.

(3) Sakai, K.; Homma, H.; Lee, J.-A.; Fukushima, T.; Santa, T.; Tashiro, K.; Iwatsubo, T.; Imai, K. Emergence of D-aspartic acid in the differentiating neurons of the rat central nervous system. *Brain Res.* **1998**, *808*, 65−71.

(4) De Rosa, A.; Mastrostefano, F.; Di Maio, A.; Nuzzo, T.; Saitoh, Y.; Katane, M.; Isidori, A. M.; Caputo, V.; Marotta, P.; Falco, G.; De Stefano, M. E.; Homma, H.; Usiello, A.; Errico, F. Prenatal expression of d-aspartate oxidase causes early cerebral d-aspartate depletion and influences brain morphology and cognitive functions at adulthood. *Amino Acids* **2020**, *52*, 597−617.

(5) Wolosker, H.; Sheth, K. N.; Takahashi, M.; Mothet, J.-P.; Brady, R. O., Jr.; Ferris, C. D.; Snyder, S. H. Purification of serine racemase: biosynthesis of the neuromodulator D-serine. *Proc. Natl. Acad. Sci. U.S.A.* **1999**, *96*, 721−725.

(6) Errico, F.; Nisticò, R.; Napolitano, F.; Mazzola, C.; Astone, D.; Pisapia, T.; Giustizieri, M.; D'Aniello, A.; Mercuri, N. B.; Usiello, A. Increased D-aspartate brain content rescues hippocampal age-related synaptic plasticity deterioration of mice. *Neurobiol. Aging* **2011**, *32*, 2229−2243.

(7) Errico, F.; Nisticò, R.; Napolitano, F.; Oliva, A. B.; Romano, R.; Barbieri, F.; Florio, T.; Russo, C.; Mercuri, N. B.; Usiello, A. Persistent increase of D-aspartate in D-aspartate oxidase mutant mice induces a precocious hippocampal age-dependent synaptic plasticity and spatial memory decay. *Neurobiol. Aging* **2011**, *32*, 2061−2074.

(8) Errico, F.; Rossi, S.; Napolitano, F.; Catuogno, V.; Topo, E.; Fisone, G.; D'Aniello, A.; Centonze, D.; Usiello, A. D-aspartate prevents corticostriatal long-term depression and attenuates schizophrenia-like symptoms induced by amphetamine and MK-801. *J. Neurosci.* **2008**, *28*, 10404−10414.

(9) Homma, H. Biochemistry of D-aspartate in mammalian cells. *Amino Acids* **2007**, *32*, 3−11.

(10) Pollegioni, L.; Sasabe, J. Editorial: Bioscience of D-amino Acid Oxidase From Biochemistry to Pathophysiology. *Front. Mol. Biosci.* **2018**, *5*, 108.

(11) Errico, F.; Napolitano, F.; Nisticò, R.; Usiello, A. New insights on the role of free D-aspartate in the mammalian brain. *Amino Acids* **2012**, *43*, 1861−1871.

(12) Affinito, O.; Scala, G.; Palumbo, D.; Florio, E.; Monticelli, A.; Miele, G.; Avvedimento, V. E.; Usiello, A.; Chiariotti, L.; Cocozza, S. Modeling DNA methylation by analyzing the individual configurations of single molecules. *Epigenetics* **2016**, *11*, 881−888.

(13) Keller, S.; Punzo, D.; Cuomo, M.; Affinito, O.; Coretti, L.; Sacchi, S.; Florio, E.; Lembo, F.; Carella, M.; Copetti, M.; Cocozza, S.; Balu, D. T.; Errico, F.; Usiello, A.; Chiariotti, L. DNA methylation landscape of the genes regulating D-serine and D-aspartate metabolism in post-mortem brain from controls and subjects with schizophrenia. *Sci. Rep.* **2018**, *8*, 10163.

(14) Cuomo, M.; Keller, S.; Punzo, D.; Nuzzo, T.; Affinito, O.; Coretti, L.; Carella, M.; de Rosa, V.; Florio, E.; Boscia, F.; Avvedimento, V. E.; Cocozza, S.; Errico, F.; Usiello, A.; Chiariotti, L. Selective demethylation of two CpG sites causes postnatal activation of the Dao gene and consequent removal of D-serine within the mouse cerebellum. *Clin. Epigenet.* **2019**, *11*, 149.

(15) Horio, M.; Ishima, T.; Fujita, Y.; Inoue, R.; Mori, H.; Hashimoto, K. Decreased levels of free D-aspartic acid in the forebrain of serine racemase (Srr) knock-out mice. *Neurochem. Int.* **2013**, *62*, 843−847.

(16) Ito, T.; Hayashida, M.; Kobayashi, S.; Muto, N.; Hayashi, A.; Yoshimura, T.; Mori, H. Serine racemase is involved in d-aspartate biosynthesis. *J. Biochem.* **2016**, *160*, 345−353.

(17) Errico, F.; Cuomo, M.; Canu, N.; Caputo, V.; Usiello, A. New insights on the influence of free d-aspartate metabolism in the mammalian brain during prenatal and postnatal life. *Biochim. Biophys. Acta, Proteins Proteomics* **2020**, *1868*, 140471.

(18) Fagg, G. E.; Matus, A. Selective association of N-methyl aspartate and quisqualate types of L-glutamate receptor with brain postsynaptic densities. *Proc. Natl. Acad. Sci. U.S.A.* **1984**, *81*, 6876−6880.

(19) Errico, F.; Nisticò, R.; Palma, G.; Federici, M.; Affuso, A.; Brilli, E.; Topo, E.; Centonze, D.; Bernardi, G.; Bozzi, Y.; D'Aniello, A.; Di Lauro, R.; Mercuri, N. B.; Usiello, A. Increased levels of d-aspartate in the hippocampus enhance LTP but do not facilitate cognitive flexibility. *Mol. Cell. Neurosci.* **2008**, *37*, 236−246.

(20) Molinaro, G.; Pietracupa, S.; Di Menna, L.; Pescatori, L.; Usiello, A.; Battaglia, G.; Nicoletti, F.; Bruno, V. D-aspartate activates mGlu receptors coupled to polyphosphoinositide hydrolysis in neonate rat brain slices. *Neurosci. Lett.* **2010**, *478*, 128−130.

(21) Krashia, P.; Ledonne, A.; Nobili, A.; Cordella, A.; Errico, F.; Usiello, A.; D'Amelio, M.; Mercuri, N. B.; Guatteo, E.; Carunchio, I. Persistent elevation of D-Aspartate enhances NMDA receptor-mediated responses in mouse substantia nigra pars compacta dopamine neurons. *Neuropharmacology* **2016**, *103*, 69−78.

(22) Keller, S.; Errico, F.; Zarrilli, F.; Florio, E.; Punzo, D.; Mansueto, S.; Angrisano, T.; Pero, R.; Lembo, F.; Castaldo, G.; Usiello, A.; Chiariotti, L. DNA methylation state of BDNF gene is not altered in prefrontal cortex and striatum of schizophrenia subjects. *Psychiatr. Res.* **2014**, *220*, 1147−1150.

(23) Errico, F.; Di Maio, A.; Marsili, V.; Squillace, M.; Vitucci, D.; Napolitano, F.; Usiello, A. Bimodal effect of D-aspartate on brain aging processes: insights from animal models. *J. Biol. Regul. Homeostatic Agents* **2013**, *27*, 49−59.

(24) Cristino, L.; Luongo, L.; Squillace, M.; Paolone, G.; Mango, D.; Piccinin, S.; Zianni, E.; Imperatore, R.; Iannotta, M.; Longo, F.; Errico, F.; Vescovi, A. L.; Morari, M.; Maione, S.; Gardoni, F.; Nisticò, R.; Usiello, A. d-Aspartate oxidase influences glutamatergic system homeostasis in mammalian brain. *Neurobiol. Aging* **2015**, *36*, 1890−1902.

https://dx.doi.org/10.1021/acs.jproteome.0c00622
J. Proteome Res. 2021, 20, 727−739

(25) Nuzzo, T.; Feligioni, M.; Cristino, L.; Pagano, I.; Marcelli, S.; Iannuzzi, F.; Imperatore, R.; D'Angelo, L.; Petrella, C.; Carella, M.; Pollegioni, L.; Sacchi, S.; Punzo, D.; De Girolamo, P.; Errico, F.; Canu, N.; Usiello, A. Free d-aspartate triggers NMDA receptor-dependent cell death in primary cortical neurons and perturbs JNK activation, Tau phosphorylation, and protein SUMOylation in the cerebral cortex of mice lacking d-aspartate oxidase activity. *Exp. Neurol.* **2019**, *317*, 51−65.
(26) Beckonert, O.; Keun, H. C.; Ebbels, T. M. D.; Bundy, J.; Holmes, E.; Lindon, J. C.; Nicholson, J. K. Metabolic profiling, metabolomic and metabonomic procedures for NMR spectroscopy of urine, plasma, serum and tissue extracts. *Nat. Protoc.* **2007**, *2*, 2692−2703.
(27) Lutz, N. W.; Beraud, E.; Cozzone, P. J. Metabolomic analysis of rat brain by high resolution nuclear magnetic resonance spectroscopy of tissue extracts. *J. Visualized Exp.* **2014**, *91*, 51829.
(28) Mo, H.; Raftery, D. Pre-SAT180, a simple and effective method for residual water suppression. *J. Magn. Reson.* **2008**, *190*, 1−6.
(29) Jacob, D.; Deborde, C.; Lefebvre, M.; Maucourt, M.; Moing, A. NMRProcFlow: A graphical and interactive tool dedicated to 1D spectra processing for NMR-based metabolomics. *Metabolomics* **2017**, *13*, 36.
(30) Govindaraju, V.; Young, K.; Maudsley, A. A. Proton NMR chemical shifts and coupling constants for brain metabolites. *NMR Biomed.* **2000**, *13*, 129−153.
(31) Sumner, L. W.; Amberg, A.; Barrett, D.; Beale, M. H.; Beger, R.; Daykin, C. A.; Fan, T. W.-M.; Fiehn, O.; Goodacre, R.; Griffin, J. L.; Hankemeier, T.; Hardy, N.; Harnly, J.; Higashi, R.; Kopka, J.; Lane, A. N.; Lindon, J. C.; Marriott, P.; Nicholls, A. W.; Reily, M. D.; Thaden, J. J.; Viant, M. R. Proposed minimum reporting standards for chemical analysis. *Metabolomics* **2007**, *3*, 211−221.
(32) Thompson, C. J.; Witt, M.; Forcisi, S.; Moritz, F.; Kessler, N.; Laukien, F. H.; Schmitt-Kopplin, P. An enhanced isotopic fine structure method for exact mass analysis in discovery metabolomics: FIA-CASI-FTMS. *J. Am. Soc. Mass Spectrom.* **2020**, *7*, 2025.
(33) Chong, J.; Soufan, O.; Li, C.; Caraus, I.; Li, S.; Bourque, G.; Wishart, D. S.; Xia, J. MetaboAnalyst 4.0: towards more transparent and integrative metabolomics analysis. *Nucleic Acids Res.* **2018**, *46*, W486−W494.
(34) Mckay, R. T. How the 1D-NOESY suppresses solvent signal in metabonomics NMR spectroscopy: An examination of the pulse sequence components and evolution. *Concepts Magn. Reson.* **2011**, *38A*, 197−220.
(35) Nicholson, J. K.; Foxall, P. J. D.; Spraul, M.; Farrant, R. D.; Lindon, J. C. 750 MHz 1H and 1H-13C NMR spectroscopy of human blood plasma. *Anal. Chem.* **1995**, *67*, 793−811.
(36) Chong, J.; Wishart, D. S.; Xia, J. Using metaboanalyst 4.0 for comprehensive and integrative metabolomics data analysis. *Curr. Protoc. Bioinf.* **2019**, *68*, No. e86.
(37) Croft, D.; Mundo, A. F.; Haw, R.; Milacic, M.; Weiser, J.; Wu, G.; Caudy, M.; Garapati, P.; Gillespie, M.; Kamdar, M. R.; Jassal, B.; Jupe, S.; Matthews, L.; May, B.; Palatnik, S.; Rothfels, K.; Shamovsky, V.; Song, H.; Williams, M.; Birney, E.; Hermjakob, H.; Stein, L.; D'Eustachio, P. The Reactome pathway knowledgebase. *Nucleic Acids Res.* **2014**, *42*, D472−D477.
(38) Goto, S.; Bono, H.; Ogata, H.; Fujibuchi, W.; Nishioka, T.; Sato, K.; Kanehisa, M. Organizing and computing metabolic pathway data in terms of binary relations. *Pac. Symp. Biocomput.* **1997**, 175−186.
(39) Kanehisa, M. Organizing and Computing Metabolic Pathway Data in Terms of Binary Relations. *Pacific Symposium on Biocomputing. Pacific Symposium on Biocomputing*; Citeseer, 1997, 175.
(40) Zhou, G.; Xia, J. Using OmicsNet for Network Integration and 3D Visualization. *Curr. Protoc. Bioinf.* **2019**, *65*, No. e69.
(41) Zhou, G.; Xia, J. OmicsNet: a web-based tool for creation and visual analysis of biological networks in 3D space. *Nucleic Acids Res.* **2018**, *46*, W514−W522.
(42) Van Veldhoven, P. P.; Mannaerts, G. P. Subcellular localization and membrane topology of sphingosine-1-phosphate lyase in rat liver. *J. Biol. Chem.* **1991**, *266*, 12502−12507.
(43) Lee, S.-E.; Lee, Y.; Lee, G. H. The regulation of glutamic acid decarboxylases in GABA neurotransmission in the brain. *Arch. Pharmacal Res.* **2019**, *42*, 1031−1039.
(44) Luján, R.; Shigemoto, R.; López-Bendito, G. Glutamate and GABA receptor signalling in the developing brain. *Neuroscience* **2005**, *130*, 567−580.
(45) Kwakowsky, A.; Schwirtlich, M.; Zhang, Q.; Eisenstat, D. D.; Erdélyi, F.; Baranyi, M.; Katarova, Z. D.; Szabó, G. GAD isoforms exhibit distinct spatiotemporal expression patterns in the developing mouse lens: correlation with Dlx2 and Dlx5. *Dev. Dyn.* **2007**, *236*, 3532−3544.
(46) Xing, L.; Huttner, W. B. J. F. i. C.; Biology, D. Neurotransmitters as Modulators of Neural Progenitor Cell Proliferation During Mammalian Neocortex Development. *Front. Cell Dev. Biol.* **2020**, *8*, 391.
(47) Represa, A.; Ben-Ari, Y. Trophic actions of GABA on neuronal development. *Trends Neurosci.* **2005**, *28*, 278−283.
(48) Addington, A. M.; Gornick, M.; Duckworth, J.; Sporn, A.; Gogtay, N.; Bobb, A.; Greenstein, D.; Lenane, M.; Gochman, P.; Baker, N.; Balkissoon, R.; Vakkalanka, R. K.; Weinberger, D. R.; Rapoport, J. L.; Straub, R. E. GAD1 (2q31.1), which encodes glutamic acid decarboxylase (GAD67), is associated with childhood-onset schizophrenia and cortical gray matter volume loss. *Mol. Psychiatr.* **2005**, *10*, 581−588.
(49) Rosenberg, D.; Artoul, S.; Segal, A. C.; Kolodney, G.; Radzishevsky, I.; Dikopoltsev, E.; Foltyn, V. N.; Inoue, R.; Mori, H.; Billard, J.-M.; Wolosker, H. Neuronal D-Serine and Glycine Release Via the Asc-1 Transporter Regulates NMDA Receptor-Dependent Synaptic Activity. *J. Neurosci.* **2013**, *33*, 3533−3544.
(50) Coyle, J. T.; Tsai, G. The NMDA receptor glycine modulatory site: a therapeutic target for improving cognition and reducing negative symptoms in schizophrenia. *Psychopharmacology* **2004**, *174*, 32−38.
(51) Li, Y.; Sacchi, S.; Pollegioni, L.; Basu, A. C.; Coyle, J. T.; Bolshakov, V. Y. Identity of endogenous NMDAR glycine site agonist in amygdala is determined by synaptic activity level. *Nat. Commun.* **2013**, *4*, 1760.
(52) Zeisel, S. H. Nutritional importance of choline for brain development. *J. Am. Coll. Nutr.* **2004**, *23*, 621S−626S.
(53) Jope, R. S. High affinity choline transport and acetylCoA production in brain and their roles in the regulation of acetylcholine synthesis. *Brain Res. Rev.* **1979**, *1*, 313−344.
(54) Miller, B. L. A review of chemical issues in 1H NMR spectroscopy: N-acetyl-L-aspartate, creatine and choline. *NMR Biomed.* **1991**, *4*, 47−52.
(55) Zeisel, S. H. Choline: critical role during fetal development and dietary requirements in adults. *Annu. Rev. Nutr.* **2006**, *26*, 229−250.
(56) Kanfer, J. N.; McCartney, D. G. Glycerophosphorylcholine phosphocholine phosphodiesterase activity of rat brain myelin. *J. Neurosci. Res.* **1989**, *24*, 231−240.
(57) Roysommuti, S.; Wyss, J. M. The Effects of Taurine Exposure on the Brain and Neurological Disorders. *Bioactive Nutraceuticals and Dietary Supplements in Neurological and Brain Disease*; Elsevier: 2015; pp 207−213.
(58) Wang, W.; Wu, Z.; Dai, Z.; Yang, Y.; Wang, J.; Wu, G. Glycine metabolism in animals and humans: implications for nutrition and health. *Amino Acids* **2013**, *45*, 463−477.
(59) Lunardi, G.; Parodi, A.; Perasso, L.; Pohvozcheva, A. V.; Scarrone, S.; Adriano, E.; Florio, T.; Gandolfo, C.; Cupello, A.; Burov, S. V.; Balestrino, M. The creatine transporter mediates the uptake of creatine by brain tissue, but not the uptake of two creatine-derived compounds. *Neuroscience* **2006**, *142*, 991−997.
(60) Snow, R. J.; Murphy, R. M. Creatine and the creatine transporter: a review. *Mol. Cell. Biochem.* **2001**, *224*, 169−181.

https://dx.doi.org/10.1021/acs.jproteome.0c00622
J. Proteome Res. 2021, 20, 727−739

(61) Juhn, M. S.; Tarnopolsky, M. Potential side effects of oral creatine supplementation: a critical review. *Clin. J. Sport Med.* **1998**, *8*, 298−304.
(62) Moffett, J.; Ross, B.; Arun, P.; Madhavarao, C.; Namboodiri, A. N-Acetylaspartate in the CNS: from neurodiagnostics to neurobiology. *Prog. Neurobiol.* **2007**, *81*, 89−131.
(63) Baslow, M. H. N-acetylaspartate in the vertebrate brain: metabolism and function. *Neurochem. Res.* **2003**, *28*, 941−953.
(64) Koller, K. J.; Zaczek, R.; Coyle, J. T. N-acetyl-aspartyl-glutamate: regional levels in rat brain and the effects of brain lesions as determined by a new HPLC method. *J. Neurochem.* **1984**, *43*, 1136−1142.
(65) Pouwels, P. J. W.; Frahm, J. Differential distribution of NAA and NAAG in human brain as determined by quantitative localized proton MRS. *NMR Biomed.* **1997**, *10*, 73−78.
(66) Jacobson, K. B. Studies on the role of N-acetylaspartic acid in mammalian brain. *J. Gen. Physiol.* **1959**, *43*, 323.
(67) Bhakoo, K. K. N-Acetyl-aspartate (NAA) metabolism. *Neural Metabolism In Vivo*; Springer, 2012; pp 1075−1093.
(68) Scherer, T.; O'Hare, J.; Diggs-Andrews, K.; Schweiger, M.; Cheng, B.; Lindtner, C.; Zielinski, E.; Vempati, P.; Su, K.; Dighe, S.; Milsom, T.; Puchowicz, M.; Scheja, L.; Zechner, R.; Fisher, S. J.; Previs, S. F.; Buettner, C. Brain insulin controls adipose tissue lipolysis and lipogenesis. *Cell Metabol.* **2011**, *13*, 183−194.
(69) López, M.; Vidal-Puig, A. Brain lipogenesis and regulation of energy metabolism. *Curr. Opin. Clin. Nutr. Metab. Care* **2008**, *11*, 483−490.
(70) Nuzzo, T.; Sacchi, S.; Errico, F.; Keller, S.; Palumbo, O.; Florio, E.; Punzo, D.; Napolitano, F.; Copetti, M.; Carella, M. J. n. S. Decreased free d-aspartate levels are linked to enhanced d-aspartate oxidase activity in the dorsolateral prefrontal cortex of schizophrenia patients. *NPJ Schizophr.* **2017**, *3*, 16.
(71) Arnold, P. D.; Sicard, T.; Burroughs, E.; Richter, M. A.; Kennedy, J. L. Glutamate transporter gene SLC1A1 associated with obsessive-compulsive disorder. *Arch. Gen. Psychiatr.* **2006**, *63*, 769−776.
(72) Deng, X.; Shibata, H.; Takeuchi, N.; Rachi, S.; Sakai, M.; Ninomiya, H.; Iwata, N.; Ozaki, N.; Fukumaki, Y. Association study of polymorphisms in the glutamate transporter genes SLC1A1, SLC1A3, and SLC1A6 with schizophrenia. *Am. J. Med. Genet., Part B* **2007**, *144B*, 271−278.
(73) Myles-Worsley, M.; Tiobech, J.; Browning, S. R.; Korn, J.; Goodman, S.; Gentile, K.; Melhem, N.; Byerley, W.; Faraone, S. V.; Middleton, F. A. Deletion at the SLC1A1 glutamate transporter gene co-segregates with schizophrenia and bipolar schizoaffective disorder in a 5-generation family. *Am. J. Med. Genet., Part B* **2013**, *162*, 87−95.
(74) Kayani, S. N.; Wilson, K. S.; Rosenberg, R. N. A Neurologic Gene Map. *Rosenberg's Molecular and Genetic Basis of Neurological and Psychiatric Disease*; Elsevier, 2015; pp 1333−1400.
(75) Rahman, S.; Footitt, E. J.; Varadkar, S.; Clayton, P. T. Inborn errors of metabolism causing epilepsy. *Dev. Med. Child Neurol.* **2013**, *55*, 23−36.
(76) Parisi, E.; Nicotera, A.; Alagna, A.; Di Rosa, G. Neonatal seizures and inborn errors of metabolism: an update. *J. Pediatr. Neonatal Care.* **2015**, *1*, 6.

https://dx.doi.org/10.1021/acs.jproteome.0c00622
J. Proteome Res. 2021, 20, 727−739